Scientific Research Publishing

Energy and Power Engineering, 2023, 15, 363-371
https://www.scirp.org/journal/epe
ISSN Online: 1947-3818
ISSN Print: 1949-243X

XPS Study of Electroless Deposited Sb_2Se_3 Thin Films for Solar Cell Absorber Material

Towhid Adnan Chowdhury

Department of Electrical & Electronic Engineering, Ahsanullah University of Science & Technology, Dhaka, Bangladesh
Email: towhid6789@yahoo.com

How to cite this paper: Chowdhury, T.A. (2023) XPS Study of Electroless Deposited Sb_2Se_3 Thin Films for Solar Cell Absorber Material. *Energy and Power Engineering*, **15**, 363-371.
https://doi.org/10.4236/epe.2023.1511021

Received: October 17, 2023
Accepted: November 14, 2023
Published: November 17, 2023

Abstract

As a thin film solar cell absorber material, antimony selenide (Sb_2Se_3) has become a potential candidate recently because of its unique optical and electrical properties and easy fabrication method. X-ray photoelectron spectroscopy (XPS) was used to determine the stoichiometry and composition of electroless Sb_2Se_3 thin films using depth profile studies. The surface layers were analyzed nearly stoichiometric. But the abundant amount of antimony makes the inner layer electrically more conductive.

Keywords

Sb_2Se_3, Electroless, Depth Profiling, Thin Film, X-Ray Photoelectron Spectroscopy

1. Introduction

Innovative photovoltaic (PV) technologies with excellent power conversion efficiency (PCE) and inexpensive mass production costs are required to expand solar energy utilization [1]. Huge research interest is developed in thin-film photovoltaic (TFPV) technologies due to the advantages of scalable flexibility, lesser material usage and greater power generation [2] [3] [4]. Important successes have been achieved in the representative cadmium telluride (CdTe) [5], copper indium gallium selenide (CIGS) [5] [6], cadmium telluride (CdTe) [7] and perovskites [8] [9] among various types of thin-film solar cells. However, the main disadvantages of these solar cells are the toxicity of cadmium (Cd), the scarcity of tellurium(Te) and indium (In) and the problem of achieving a stoichiometric ratio. As a result, different novel earth-abundant materials, such as $CuSbSe_2$ [10], Cu_2SnS_3 [11], $Cu_2ZnSnSe_4$ [12], SnSe [13], $CuSbS_2$ [14], Sb_2S_3 [15] and Sb_2Se_3 [16] have been suggested as a substitute for the low cost and eco-friendly of thin film

solar cells.

Among those, antimony selenide (Sb_2Se_3) has emerged as a promising candidate for next-generation solar absorber material. It is a compound semiconductor belonging to the group V-VI with a suitable band gap of 1.1 - 1.2 eV and finds widespread applications in optoelectronic, thermoelectric photoconducting targets, infrared spectroscopy and television camera [17] [18]. It was used in the 1950s [19] in mineral anti-monselite [20]. It exhibits good photovoltaic and thermoelectric properties which allow possible usage for thermophotovoltaic, thermoelectric [21] [22] [23] [24] and solar cells [25]. Sb_2Se_3 also finds usage in batteries, photodetectors, and memory gadgets [26]. Tremendous research has been focused on Sb_2Se_3 for hybrid solar cell fabrication as light absorber materials [21] [27] due to its low cost, narrow band gap, non-toxic and comparatively earth-abundant [28]. In the present work, electroless deposition of Sb_2Se_3 thin films was done and examination of stoichiometry of Sb_2Se_3 thin films using X-ray photoelectron spectroscopy (XPS) depth profiling was carried out.

2. Experimental Details

All the glassware in our experiment has been cleaned by first washing and scrubbing with Alconox, followed by a 20 min. sonication in acetone, and methanol, and then washed with isopropanol and DI water. Afterward, the glassware was dried using N_2 gas. An aqueous solution of 0.227 g Sb_2Se_3, 0.259 g Na_2SeO_3, 3 ml hydrazine hydrate and 50 ml water have been used for precursor solution electroless deposition. The substrate temperature was controlled by a hot plate with which a thermocouple was attached. The substrate temperature was maintained within ±1˚C of 40˚C for 50 min.

The composition of the Sb_2Se_3 thin film was studied using XPS. The XPS spectra were obtained by using monochromatic Al Kα radiation (1486.6 eV). through a Kratos AXIS Ultra DLD XPS system at a base pressure of 5×10^{-10} Torr, equipped with an electronic neutralization gun to eliminate the charge effect on the sample surface. The sample was firstly pressed to a 1 × 13 mm disc and fixed to the sample holder, and then it was degassed in the load lock chamber overnight. After that, it was removed to the test chamber for XPS study. All binding energy values were calibrated by using the value of contaminant carbon (C 1s 284.6 eV) as a reference. The sample was then ion sputtered with Ar^+ at 4000 eV and 15 mA for 1 min and 10 min.

XPSPeak software version 4.1 was used to obtain all the spectra. The spectra were deconvoluted using a mixture of Lorentzian-Gaussian type peaks.

3. Results and Discussion

The chemical purity and the composition of Sb_2Se_3 thin films were investigated by XPS analysis. The typical XPS survey spectrum Sb_2Se_3 is shown in **Figure 1(a)**. The peaks arising from Sb 3p, 3d, Sb Auger, Na 1s, Na Auger, C 1s, Se 3p and 3d are clearly seen in the spectrum. Carbon contamination is present in almost

all the preparations. All other peaks that arise due to energy loss features on the major peaks are weak and broad. The Se 3d intensity is very large compared to the Se 3p intensity, and that is why we have reported just the Se 3d spectra of Se compounds. High-resolution spectra of the Sb 3d core level and Se 3d core level are shown in **Figure 1(b)** and **Figure 1(c)** respectively. The two peaks at 530.1 eV and 539.4 eV can be assigned to the binding energy of Sb $3d_{5/2}$ and $3d_{3/2}$ respectively. The separation of Sb 3d doublet is by 9.3 eV. These binding energy values of Sb 3d are characteristic of antimony tri-selenide [18]. No oxygen peak was observed in this hydrazine-processed Sb_2Se_3 thin film in the high-resolution spectra of the Sb 3d core level. The binding energy value of 54.96 eV of Se 3d is characteristic of antimony tri-selenide [18].

The XPS survey spectrum of Sb_2Se_3 thin film after 1 min. Ar^+ ion sputtering is shown in **Figure 2(a)**. The peaks arising from Sb 3p, 3d, Sb Auger, Na 1s, Na Auger, C 1s, Se 3p and 3d are clearly seen in the spectrum. Carbon contaminations on the surface were reduced significantly after 1 min. Ar^+ ion sputtering. High resolution spectra of Sb 3d core level and Se 3d core level are shown in the

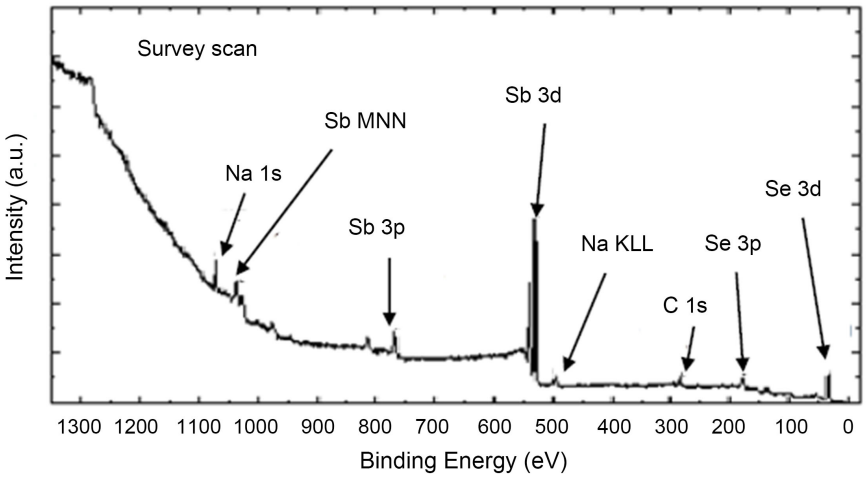

(a)

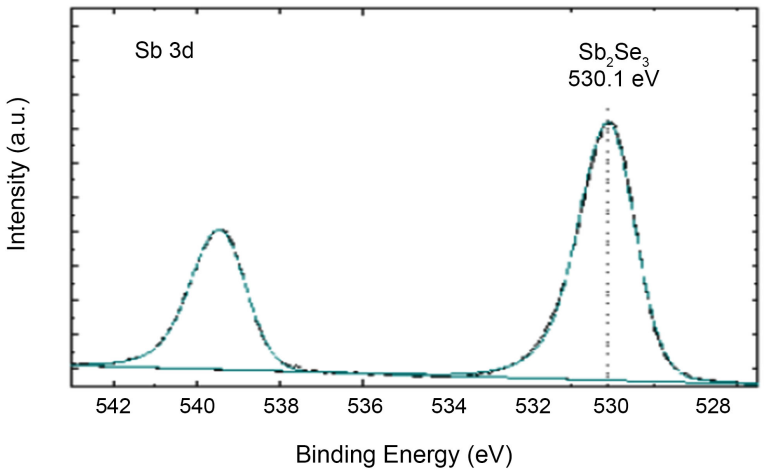

(b)

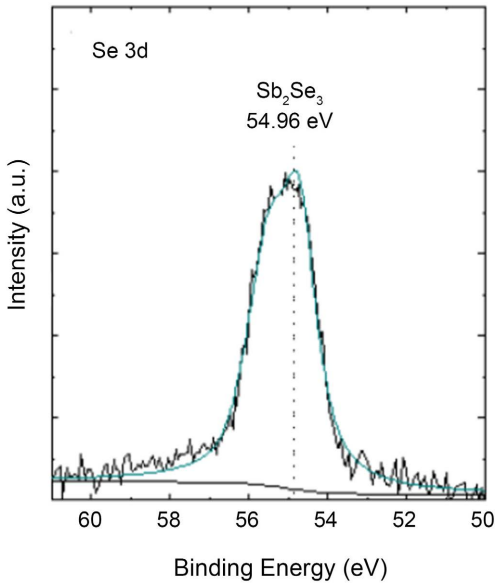

(c)

Figure 1. (a) XPS survey spectrum of as-deposited Sb_2Se_3 film. (b) High resolution XPS spectra of the Sb 3d core level of as-deposited Sb_2Se_3 film. (c) High resolution XPS spectra of the S 2p core level of as-deposited Sb_2Se_3 film.

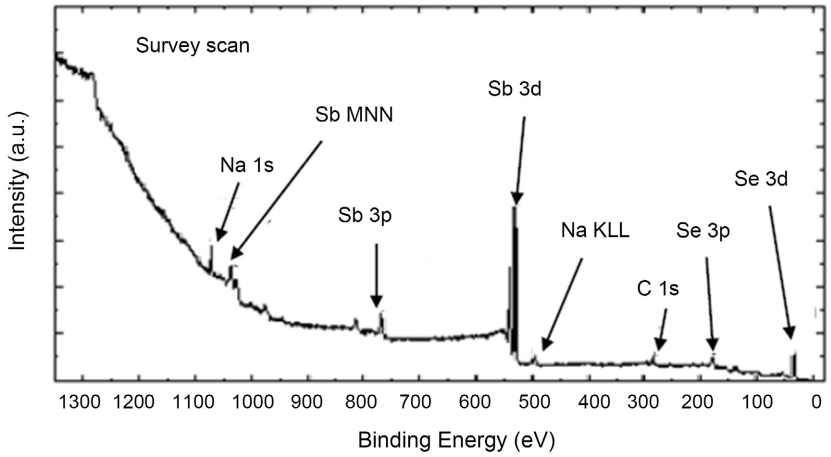

(a)

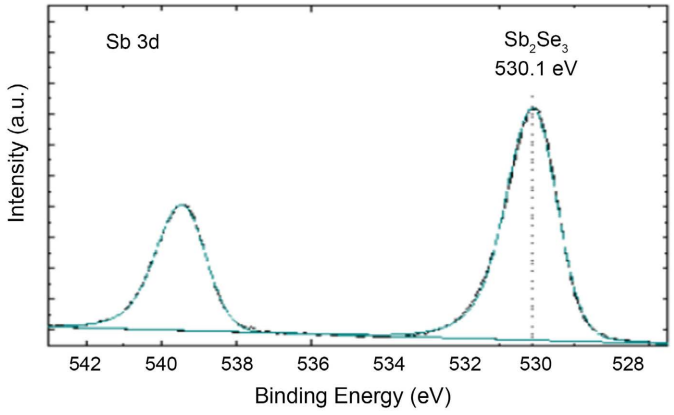

(b)

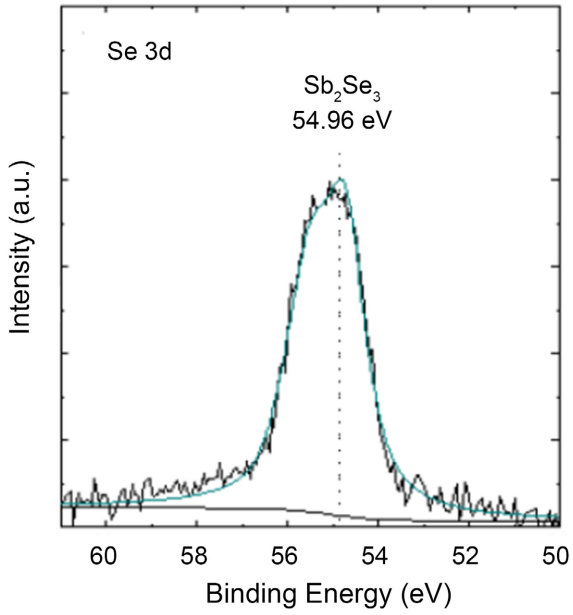

(c)

Figure 2. (a) XPS survey spectrum of Sb_2Se_3 film after 1 min. Ar^+ ion sputtering. (b) High resolution XPS spectra of the Sb 3d core level of Sb_2Se_3 film after 1 min. Ar^+ ion sputtering. (c) High resolution XPS spectra of the Se 3d core level of Sb_2Se_3 film after 1 min. Ar^+ ion sputtering.

Figure 2(b) and **Figure 2(c)** respectively. The two peaks at 530.1 eV and 539.4 eV can be assigned to the binding energy of Sb $3d_{5/2}$ and $3d_{3/2}$ respectively. The separation of Sb 3d double is by 9.3 eV. These binding energy values of Sb 3d are characteristic of antimony tri-selenide [18]. No oxygen peak was observed in this hydrazine-processed Sb_2Se_3 thin film in the high-resolution spectra of the Sb 3d core level. The binding energy value of 54.96 eV of Se 3d is characteristic of antimony tri-selenide [18]. No chemical shift was observed in Sb 3d and Se 3d core levels after 1 min. of Ar^+ ion sputtering.

The XPS survey spectrum of Sb_2Se_3 thin film after 10 min. Ar^+ ion sputtering is shown in **Figure 3(a)**. The peaks arising from Sb 3p, 3d, Sb Auger, Na 1s, C 1s, Se 3p and 3d are clearly seen in the spectrum. Carbon contaminations and the peak corresponding to Na 1s core level were reduced to a low level after 10 min. Ar^+ ion sputtering. High-resolution spectra of the Sb 3d core level and Se 3d core level are shown in **Figure 3(b)** and **Figure 3(c)** respectively. The two peaks at 530.2 eV and 539.5 eV can be assigned to the binding energy of Sb $3d_{5/2}$ and $3d_{3/2}$ respectively. The separation of Sb 3d double is by 9.3 eV. These binding energy values of Sb 3d are characteristic of antimony tri-selenide [18]. No oxygen peak was observed in this hydrazine-processed Sb_2Se_3 thin film in the high-resolution spectra of the Sb 3d core level. The binding energy value of 54.96 eV of the Se 3d is characteristic of antimony tri-selenide [18]. The binding energy value of the Sb 3d core level is increased by 0.1 eV and no chemical shift was observed in the Se 3d core level after 10 min. of Ar^+ ion sputtering.

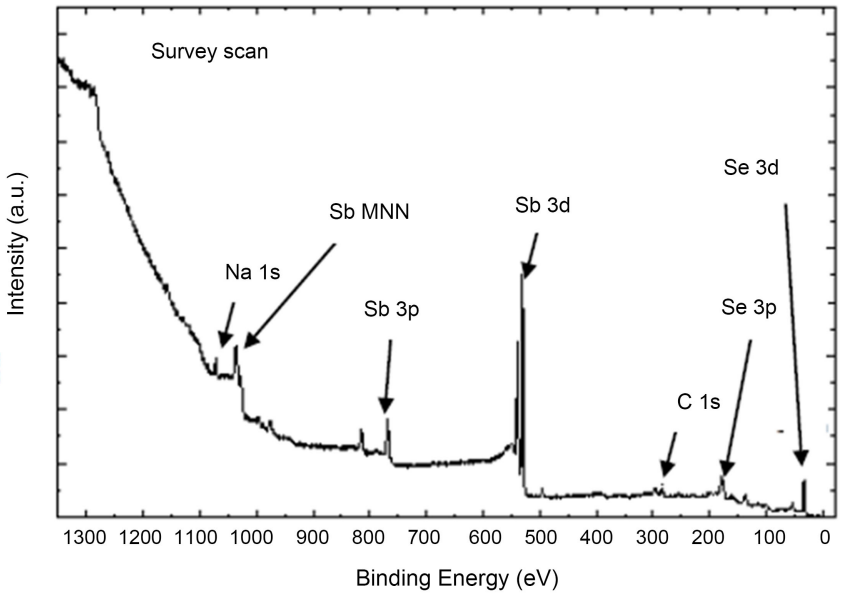

(a)

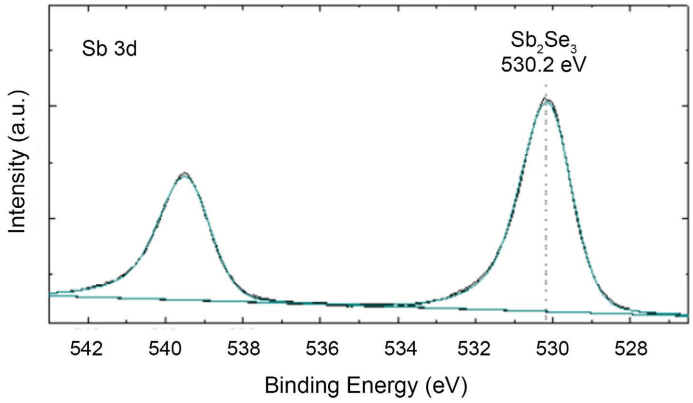

(b)

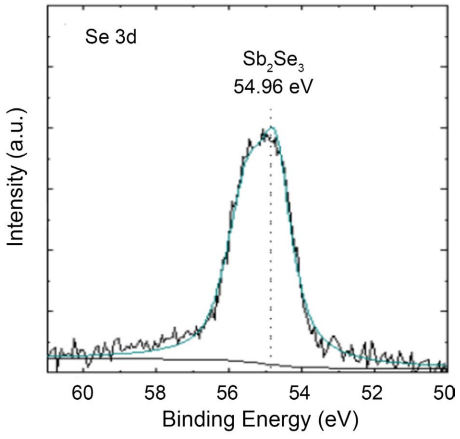

(c)

Figure 3. (a) XPS survey spectrum of Sb_2Se_3 film after 10 min. Ar^+ ion sputtering. (b) High resolution XPS spectra of the Sb 3d core level of Sb_2Se_3 film after 10 min. Ar^+ ion sputtering. (c) High resolution XPS spectra of the Se 3d core level of Sb_2Se_3 film after 10 min. Ar^+ ion sputtering.

4. Conclusion

The device performance deteriorates due to the presence of recombination centers created by oxygen impurity [18]. Oxygen can be present in Sb_2Se_3 thin films as it is air-sensitive. So X-ray photoelectron spectroscopy (XPS) was used to investigate the composition of Sb_2Se_3 thin film. Almost stoichiometric composition of Sb_2Se_3 thin films close to the surface is observed using the XPS depth profile result in this work. The peak intensity of C(1s) becomes smaller at the deeper surface as sputter time is increased. No oxygen peak was observed in this hydrazine-processed Sb_2Se_3 thin film in the high-resolution spectra of the Sb 3d core level which is good for device performance. The peak corresponding to Na 1s core level decreased significantly with Ar^+ ion sputtering time. The Sb 3d core level binding energy is increased by 0.1 eV after 10 min Ar^+ ion sputtering. No chemical shift was observed in the Se 3d core level during Ar^+ ion sputtering.

Acknowledgements

The work was supported by the Advanced Support Program for Innovative Research Excellence-(ASPIRE-I), grant number 15530-E404 and Support to Promote Advancement of Research and Creativity (SPARC), grant number 15530-E413 of the University of South Carolina, Columbia, USA.

Conflicts of Interest

The author declares no conflicts of interest regarding the publication of this paper.

References

[1] Wang, W., Cao, Z., Wu, L., Chen, G., Ao, J., Luo, J. and Zhang, Y. (2022) Interface Etching Leads to the Inversion of the Conduction Band Offset between the CdS/Sb_2Se_3 Heterojunction and High-Efficient Sb_2Se_3 Solar Cells. *ACS Applied Energy Materials*, **5**, 2531-2541. https://doi.org/10.1021/acsaem.1c04078

[2] Liang, G., Chen, M., Ishaq, M., Li, X., Tang, R., Zheng, Z., Su, Z., Fan, P., Zhang, X. and Chen, S. (2022) Crystal Growth Promotion and Defects Healing Enable Minimum Open-Circuit Voltage Deficit in Antimony Selenide Solar Cells. *Advanced Science*, **9**, Article ID: 2105142. https://doi.org/10.1002/advs.202105142

[3] Wang, W., Wang, X., Chen, G., Yao, L., Huang, X., Chen, T., Zhu, C., Chen, S., Huang, Z. and Zhang, Y. (2019) Over 6% Certified $Sb_2(S, Se)_3$ Solar Cells Fabricated Via *in situ* Hydrothermal Growth and Postselenization. *Advanced Electronic Materials*, **5**, Article ID: 1800683. https://doi.org/10.1002/aelm.201800683

[4] Chen, S., Zheng, Z., Cathelinaud, M., Ma, H., Qiao, X., Su, Z., Fan, P., Liang, G., Fan, X. and Zhang, X. (2019) Magnetron Sputtered Sb_2Se_3-Based Thin Films towards High Performance Quasi-Homojunction Thin Film Solar Cells. *Solar Energy Materials and Solar Cells*, **203**, Article ID: 110154. https://doi.org/10.1016/j.solmat.2019.110154

[5] Kaelin, M., Rudmann, D. and Tiwari, A.N. (2004) Low Cost Processing of CIGS Thin Film Solar Cells. *Solar Energy*, **77**, 749-756. https://doi.org/10.1016/j.solener.2004.08.015

[6] Islam, M.M., Ishizuka, S., Yamada, A., Sakurai, K., Niki, S., Sakurai, T. and Akimoto, K. (2009) CIGS Solar Cell with MBE-Grown ZnS Buffer Layer. *Solar Energy Materials and Solar Cells*, **93**, 970-972. https://doi.org/10.1016/j.solmat.2008.11.047

[7] Guillermo, H., Rimmaudo, I., Riech, I., Abelenda, A. and López-Sánchez, A. (2022) A Simple Model for Studying the Effects of Activation Treatment on the Defects Structure of Cadmium Telluride Solar Cells. *Optik*, **262**, Article ID: 169296. https://doi.org/10.1016/j.ijleo.2022.169296

[8] Green, M.A., Dunlop, E., Hohl-Ebinger, J., Yoshita, M., Kopidakis, N. and Hao, X. (2021) Solar Cell Efficiency Tables (Version 57). *Progress in Photovoltaics*, **29**, 3-15. https://doi.org/10.1002/pip.3371

[9] Bouich, A., Marí-Guaita, J., Sahraoui, B., Palacios, P. and Marí, B. (2022) Tetrabutylammonium (TBA)-Doped Methylammonium Lead Iodide: High Quality and Stable Perovskite Thin Films. *Frontiers in Energy Research*, **10**, Article ID: 840817. https://doi.org/10.3389/fenrg.2022.840817

[10] Xue, D.J., Yang, B., Yuan, Z.K., Wang, G., Liu, X., Zhou, Y., Hu, L., Pan, D., Chen, S. and Tang, J. (2015) $CuSbSe_2$ as a Potential Photovoltaic Absorber Material: Studies from Theory to Experiment. *Advanced Energy Materials*, **5**, Article ID: 1501203. https://doi.org/10.1002/aenm.201501203

[11] Chantana, J., Uegaki, H. and Minemoto, T. (2017) Influence of Na in Cu_2SnS_3 Film on Its Physical Properties and Photovoltaic Performances. *Thin Solid Films*, **636**, 431-437. https://doi.org/10.1016/j.tsf.2017.06.044

[12] Hartnauer, S., Korbel, S., Marques, M.A.L., Botti, S., Pistor, P. and Scheer, R. (2016) Research Update: Stable Single-Phase Zn-Rich $Cu_2ZnSnSe_4$ through in Doping. *APL Materials*, **4**, Article ID: 070701. https://doi.org/10.1063/1.4953435

[13] Razykov, T.M., Boltaev, G.S., Bosio, A., Ergashev, B., Kouchkarov, K.M., Mamarasulov, N.K., Mavlonov, A.A., Romeo, A., Romeo, N., Tursunkulov, O.M. and Yuldoshov, R. (2018) Characterisation of SnSe Thin Films Fabricated by Chemical Molecular Beam Deposition for Use in Thin Film Solar Cells. *Solar Energy*, **159**, 834-840. https://doi.org/10.1016/j.solener.2017.11.053

[14] Septina, W., Ikeda, S., Iga, Y., Harada, T. and Matsumura, M. (2014) Thin Film Solar Cell Based on $CuSbS_2$ Absorber Fabricated from an Electrochemically Deposited Metal Stack. *Thin Solid Films*, **550**, 700-704. https://doi.org/10.1016/j.tsf.2013.11.046

[15] Tang, R., Wang, X., Jiang, C., Li, S., Jiang, G., Yang, S., Zhu, C. and Chen, T. (2018) Vacuum Assisted Solution Processing for highly Efficient Sb_2S_3 Solar Cells. *Journal of Materials Chemistry A*, **6**, 16322-16327. https://doi.org/10.1039/C8TA05614E

[16] Tang, R., Zheng, Z.H., Su, Z.H., Li, X.J., Wei, Y.D., Zhang, X.H., Fu, Y.Q., Luo, J.T., Fan, P. and Liang, G.X. (2019) Highly Efficient and Stable Planar Heterojunction Solar Cell Based on Sputtered and Post-Selenized Sb_2Se_3 Thin Film. *Nano Energy*, **64**, Article ID: 103929. https://doi.org/10.1016/j.nanoen.2019.103929

[17] Zhou, Y., Leng, M., Xia, Z., Zhong, J., Song, H., Liu, X., Yang, B., Zhang, J., Chen, J., Zhou, K., Han, J., Cheng, Y. and Tang, J. (2014) Solution-Processed Antimony Selenide Heterojunction Solar Cells. *Advanced Energy Materials*, **4**, Article ID: 1301846. https://doi.org/10.1002/aenm.201301846

[18] Liu, X., Chen, J., Luo, M., Leng, M., Xia, Z., Zhou, Y., Qin, S., Xue, D., Lv, L., Huang, H., Niu, D. and Tang, J. (2014) Thermal Evaporation and Characterization of Sb_2Se_3 Thin Film for Substrate Sb_2Se_3/CdS Solar Cells. *ACS Applied Materials & Interfaces*, **6**, 10687-10695. https://doi.org/10.1021/am502427s

[19] Donges, E. (1950) Uber Selenohalogenide Des Dreiwertigen Antimons und Wis-

muts und Uber Antimon(III)-Selenid. *Zeitschrift für anorganische und allgemeine*, **263**, 280-291. https://doi.org/10.1002/zaac.19502630508

[20] Jiajun, L., Jianming, L., Congqiang, L., Wenquan, L., Shirong, L. and Wenchao, S. (1999) Mineralogy of the Stibnite-Antimonselite Series. *International Geology Review*, **41**, 1042-1050. https://doi.org/10.1080/00206819909465189

[21] Black, J., Conwell, E.M., Seigle, L. and Spencer, C.W. (1957) Electrical and Optical Properties of Some M2v-bN3vi-b Semiconductors. *Journal of Physics and Chemistry of Solids*, **2**, 240-251. https://doi.org/10.1016/0022-3697(57)90090-2

[22] Rosi, F.D., Abeles, B. and Jensen, R.V. (1959) Materials for Thermoelectric Refrigeration. *Journal of Physics and Chemistry of Solids*, **10**, 191-200. https://doi.org/10.1016/0022-3697(59)90074-5

[23] Jeffrey, S.G. and Toberer, E.S. (2008) Complex Thermoelectric Materials. *Nature Materials*, **7**, 105-114. https://doi.org/10.1038/nmat2090

[24] Fourspring, P.M., DePoy, D.M., Rahmlow, T.D., Wa-semand, J.E.L. and Gratrix, E.J. (2006) Optical Coatings for Thermophotovoltaic Spectral Control. *Applied Optics*, **45**, 1356-1358. https://doi.org/10.1364/AO.45.001356

[25] Zhou, B. and Zhu, J. (2009) Microwave-Assisted Synthesis of Sb_2Se_3 Submicro Rods, Compared with Those of Bi_2Te_3 and Sb_2Te_3. *Nanotechnology*, **20**, Article ID: 085604. https://doi.org/10.1088/0957-4484/20/8/085604

[26] Mamta, Singh, Y., Maurya, K.K. and Singh, V.N. (2021) A Review on Properties, Applications, and Deposition Techniques of Antimony Selenide. *Solar Energy Materials and Solar Cells*, **230**, Article ID: 111223. https://doi.org/10.1016/j.solmat.2021.111223

[27] Chang, J.A., Rhee, J.H., Im, S.H., Lee, Y.H., Kim, H.J., Seok, S.I., Nazeeruddin, M.K. and Gratzel, M. (2010) High-Performance Nanostructured Inorganic-Organic Heterojunction Solar Cells. *Nano Letters*, **10**, 2609-2612. https://doi.org/10.1021/nl101322h

[28] Arun, P., Vedeshwar, A.G. and Mehra, N.C. (1999) Laser-Induced Crystallization in Amorphous Films of Sb_2C_3 (C = S, Se, Te), Potential Optical Storage Media. *Journal of Physics D: Applied Physics*, **32**, 183-190. https://doi.org/10.1088/0022-3727/32/3/001